UC San Diego
UC San Diego Previously Published Works

Title

Sonar estimates of daytime activity levels of Euphausia pacifica in Saanich Inlet

Permalink

https://escholarship.org/uc/item/78j4061n

Journal

Canadian Journal of Fisheries and Aquatic Sciences, 56(11)

ISSN

0706-652X

Authors

Jaffe, Jules S
Ohman, Mark D
De Robertis, Alex

Publication Date

1999-11-01

DOI

10.1139/f99-132

Peer reviewed

Sonar estimates of daytime activity levels of *Euphausia pacifica* in Saanich Inlet

Jules S. Jaffe, Mark D. Ohman, and Alex De Robertis

Abstract: A three-dimensional multibeam tracking sonar system (FishTV) was deployed in the stratified waters of Saanich Inlet in July–August of 1996 and 1997 to assess the swimming behavior of euphausiids in situ. Here, a new algorithm is used to estimate swimming velocities of animals from the uncorrelated displacements of acoustic targets in pairs of sonar frames with increasing time delays between frames. Assuming isotropic motions of euphausiids, the superior spatial resolution of the sonar in one dimension (range) is used to infer the three-dimensional motions. We applied the algorithm to sonar tracks of groups of 10 000 – 25 000 euphausiids recorded in the daytime at depths just above the oxycline on six different occasions. The animal movements were described with a probability density function for velocity which suggests that about 60–70% of the animals were moving less than or equal to 0.3–1.2 cm·s^{-1}. These distributions imply remarkably low swimming speeds and quiescent behavior. Limited motility in the daytime would confer two major advantages on the euphausiids: reduction of encounter rates with ambush predators and decreased metabolic costs.

Résumé : Nous avons déployé un système de pistage tridimensionnel par sonar multifaisceaux (FishTV) dans les eaux stratifiées du bras Saanich en juillet-août 1996 et 1997 pour examiner in situ le comportement de nage des euphausiacés. Nous utilisons ici un nouvel algorithme pour estimer les vitesses de nage des animaux à partir des déplacements non corrélés de cibles acoustiques dans des paires de clichés sonar en faisant croître l'intervalle entre les clichés. En supposant que les déplacements des euphausiacés sont isotropes, nous nous sommes servis de la résolution spatiale supérieure du sonar dans une seule dimension (la portée) pour inférer les déplacements dans les trois dimensions. Nous avons appliqué l'algorithme aux tracés sonar de groupes de 10 000 à 25 000 euphausiacés enregistrés à six occasions différentes, de jour, à des profondeurs juste supérieures à l'oxycline. Les déplacements des animaux ont été décrits avec une fonction de densité pour la vitesse qui permet de penser que 60 à 70% des animaux se déplaçaient à une vitesse inférieure ou égale à $0,3$–$1,2$ cm·s^{-1}. Ces distributions correspondent à des vitesses remarquablement basses et à un comportement passif. Leur motilité réduite pendant le jour peut conférer deux grands avantages aux euphausiacés : réduction des taux de rencontre avec des prédateurs à l'affût, et baisse des dépenses métaboliques.

[Traduit par la Rédaction]

Introduction

Euphausiid crustaceans are distributed throughout the World Ocean (Brinton et al. 1999) and in many localities are dominant components of marine food webs. Owing to their relatively large body size, they are disproportionately significant as prey items for a variety of marine planktivores. Quantitative models of euphausiid bioenergetics, encounter rates with prey and predators, bioenergetics, and diel vertical migrations are dependent upon knowledge of a variety of behavioral characteristics, most of which remain poorly known. None have been determined for individual euphausiids in their natural habitat. In this article, we report measurement of the daytime activity level of *Euphausia pacifica* at depth in Saanich Inlet, British Columbia. To our knowledge, this study is the first quantitative assessment of the swimming speeds of individual euphausiids in situ.

J.S. Jaffe,[1] M.D. Ohman, and A. De Robertis. Scripps Institution of Oceanography, La Jolla, CA 92093, U.S.A.

[1]Author to whom all correspondence should be addressed. e-mail: jules@mpl.ucsd.edu

The ability to formulate sensible models for prey–predator encounter, individual somatic growth, and growth of populations rests upon knowledge of natural behavior. For example, among the more important parameters for encounter models are prey and predator swimming velocities and local prey densities (e.g., Gerritsen and Strickler 1977; Buskey et al. 1993). Therefore, diel variations in swimming velocity and in formation and dispersion of local prey patches can markedly affect computations of encounter rates. Similarly, bioenergetic growth models require accurate knowledge of metabolic losses. Since the metabolic rate of euphausiids is known to depend steeply upon the swimming speed of the animals (Torres and Childress 1983), it is essential to understand natural swimming speeds and activity levels of euphausiids. Some models assume negligible swimming speeds of euphausiids when they are at daytime depths (Andersen and Nival 1991), but this has never been measured and remains an important unknown quantity.

With the recent development of FishTV (Jaffe et al. 1995) and the combined OASIS (optical–acoustic submersible imaging system) system (Jaffe et al. 1998), we now have the capability for both tracking and identifying individual zooplankton in situ. The system can be used to measure the abundance of zooplankton by counting the number of reflec-

Fig. 1. Image created by averaging the acoustic returns from the inner four beams of the sonar system as a function of range and time. The data were contoured as a fraction of the maximum target strength (about –67 dB) with the black values corresponding to targets that were within 5% of this value.
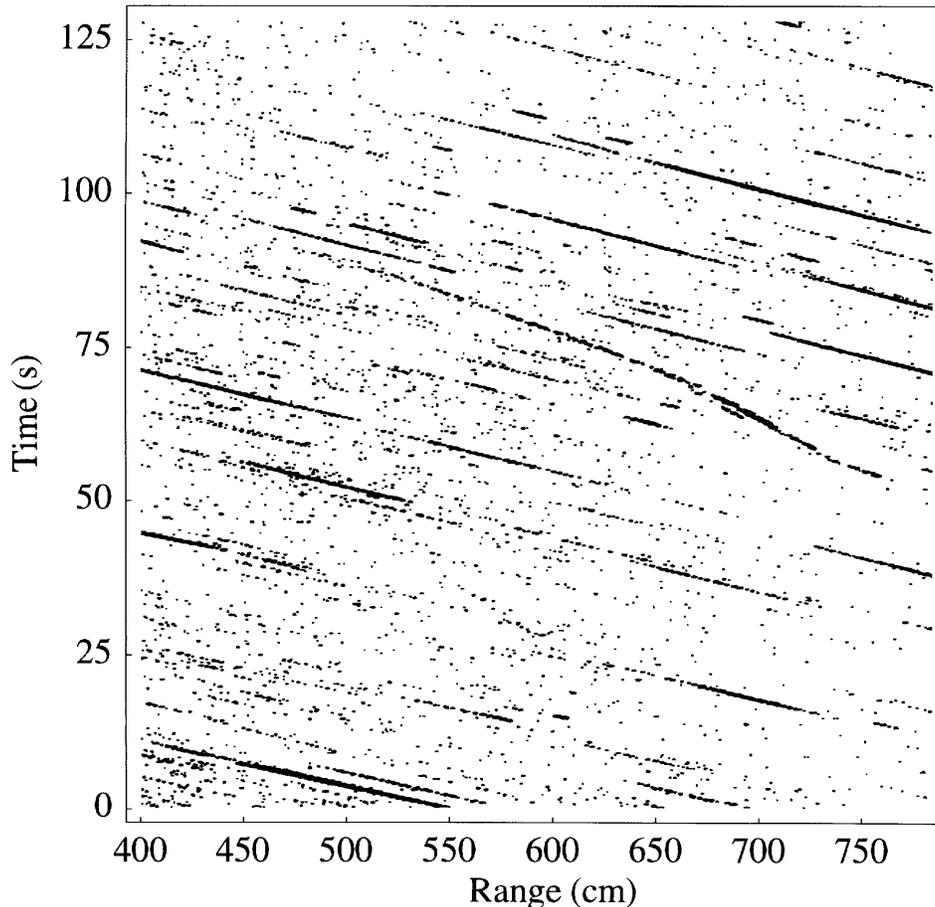
tions in the insonified volume from individual animals. The intensity of the reflections can then be used to obtain the animals' target strength. Three-dimensional locations of animals are determined that can then be linked together in successive frames to form three-dimensional trajectories (McGehee and Jaffe 1996). Briefly, the OASIS system consists of a sensitive CCD camera, a set of current meters, and the FishTV system, mounted on a large current vane that is oriented so that in even moderate current (1–5 cm·s^{-1}), the sonar is pointing into the current. Observations of animal trajectories indicated that there was no detectable behavioral response to the presence of OASIS (Jaffe et al. 1998), as the device was downstream from the animals and data collection started at a range of 2 meters from the transducers.

As a study site for our investigations, we chose Saanich Inlet in British Columbia. Saanich Inlet is a fjord with an oxygenated surface layer and seasonally anoxic bottom waters, with a large resident population of *E. pacifica* (Boden and Kampa 1965). In midsummer, horizontal advection and vertical shear are relatively modest, apart from episodes of strong winds and tidal mixing associated with spring tidal cycles. Visual observations (Mackie and Mills 1983) from the *Pisces IV* submersible in Saanich Inlet indicated that *E. pacifica* aggregates immediately above the oxycline.

Methods and materials

Experimental considerations

These studies were conducted in two consecutive summers (1996 and 1997) during 2 weeks in late July and early August. An initial CTD-O$_2$ survey along the central axis of the fjord was used to measure the depth of the anoxic layer. Based on these measurements, a site was chosen (48°34.4′N, 123°30.4′W) where euphausiids aggregated at a depth of about 70–90 m during the daytime. This depth was chosen to be slightly shallower than the present operational depth capability of the OASIS system. The OASIS system, which was deployed in both a vertical profiling mode and at several fixed depths, provided vertical distribution patterns of euphausiids that were consistent with those derived from MOCNESS tows (A. De Robertis, unpublished data).

Briefly, the FishTV system is a multibeam sonar system that operates at a frequency of 445 kHz and at frame rates of up to 4 Hz. The system provides acoustic backscatter from a set of 64 beams whose beam widths are 2 × 2°. The system resolves 512 range bins at a range increment of 0.75 cm, which yields a three-dimensional data set of dimensions 16° × 16° × 3.8 m. Extensive target strength determinations done recently with live euphausiids (A. De Robertis, unpublished data) indicate that, on average, the system can resolve animals down to a body length of 7–10 mm under the system parameters used for this set of observations.

The present study is based on six extended deployments at a

Fig. 2. Simulation of the trajectories of 100 targets as a function of time. The targets were assigned uniformly distributed starting positions initially in a 10 × 10 unit area and then translated by an amount that was the superposition of a uniform current to the right and a normally distributed velocity distribution whose standard deviation was 0.25 distance unit per time interval. Shown are the positions of the targets at delays of (*a*) one, (*b*) two, (*c*) three, and (*d*) four time intervals ($\triangle T$) and (*e*) the underlying probability density functions for each set of horizontal movements.
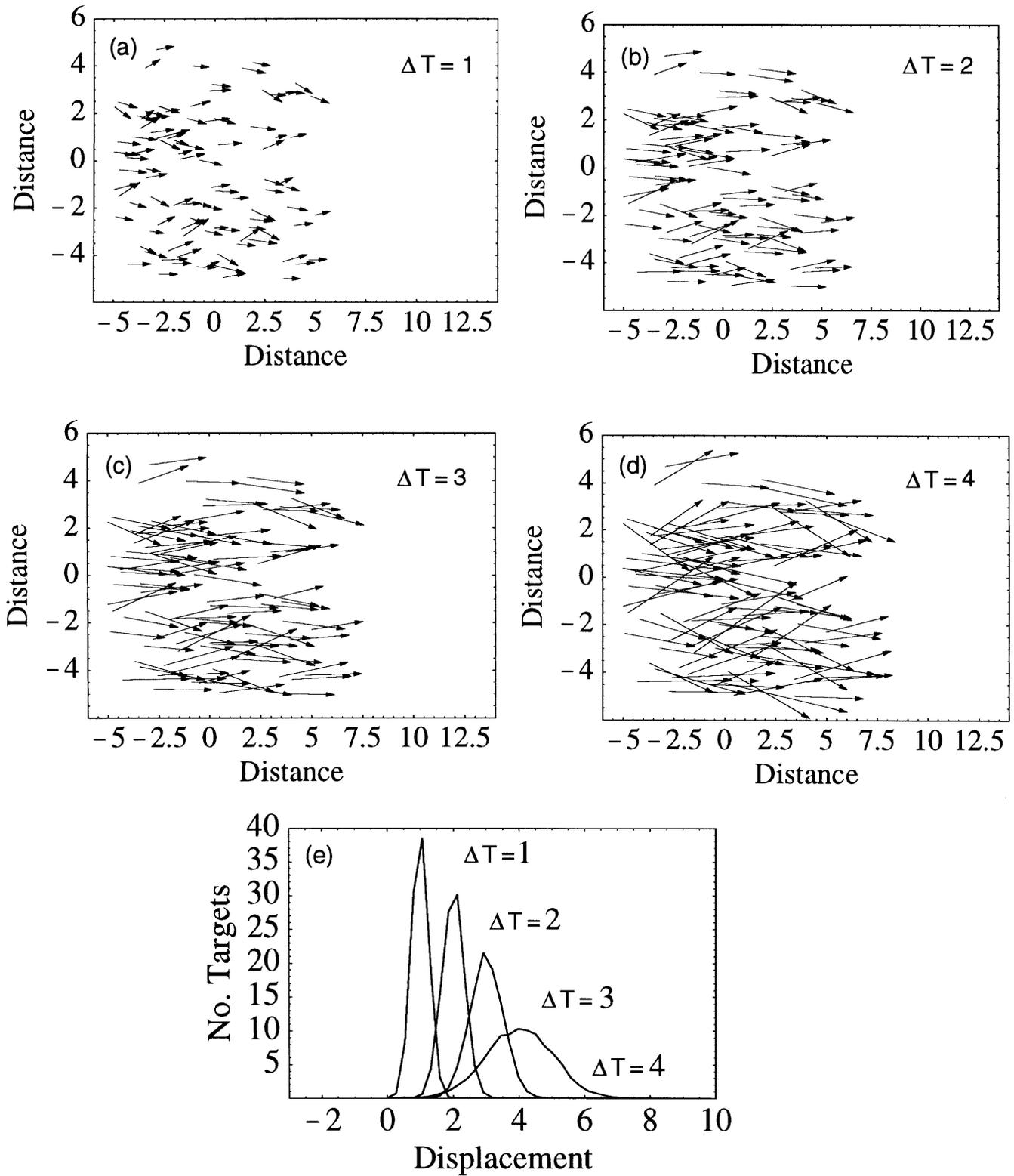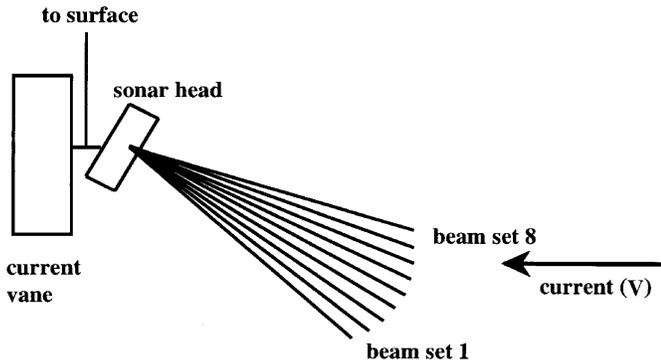
Fig. 3. Schematic illustration of the geometric arrangement of the FishTV transducers and current vane during deployment. Each projected beam is received by eight transducers.

Fig. 4. Set of displacement distribution functions (the number of targets that underwent translation Δx in time interval ΔT as a function of time delay and beam set for the data collected on 31 July 1996. (*a*) Beam set 1 is the set of eight beams that are pointing most downward and (*b*) beam set 8 is the set of beams that are oriented the most horizontally.

fixed depth in the daytime aggregation layer, four in 1996 and two in 1997 (see Table 1). Several thousand frames of animal sound reflection were collected in each session with up to hundreds of animals in each. The OASIS system was deployed at a stationary depth of 70–90 m for intervals of 5–30 min during the daytime. For this study, a set of six runs were used, four from the summer of 1996 and two from the summer of 1997. During 1996 the sonar was operated at a rate of 2 Hz and in 1997 at 4 Hz. During 1996 the sonar acquired data starting at a range of 1.9 m and ending at a range of 5.7 m. In 1997, the sonar acquired data starting at a range of 4 m and ending at a range of 7.8 m. We chose to use only a subset of these animal trajectories, the strongest 20 acoustic targets in each frame, to insure that the same individuals were detected in successive frames. The number of animals that were tracked was a decreasing function of the length of observation time, with about 25 000 animals tracked for the shortest time intervals (0.25–0.5 s) to about 10 000 animals tracked for the longest intervals (2–4 s).

Mathematical considerations

Consideration of the sonar geometry and its anisotropic resolution in three dimensions motivated the development of a special algorithm to detect small motions. Both the motivation for this algorithm and the theoretical basis for its performance are considered in this section.

As an example of the problem encountered, consider that the azimuthal resolution of the system is 2 × 2°. At a range of 3 m, this results in a resolution of 10.5 × 10.5 cm across the beam. In contrast, the range resolution of the system, which is dictated by the bandwidth of the signal, is about 1 cm. Since the animal motions were suspected to be small (see below), an algorithm was developed that makes use of this much greater range resolution.

An image containing the tracks of many animals is illustrated in Fig. 1. It was derived by taking the range-varying intensity of the average backscatter of the inner four acoustic beams and displaying it as a function of time. The figure shows many dark diagonal lines of high acoustic reflectivity that can be interpreted as animals that are drifting towards the device. Since the sonar is pointed into the current, the drift is at a constant rate. The parallel lines in Fig. 1 suggest that the observed motions are primarily due to drift and not due to animal swimming. On the other hand, several trajectories show animal motions that are not "going with the flow" and can be interpreted as swimming. Animal trajectories also seem to appear and disappear. Whether these starts and ends are due to the animals going outside the inner four beams or perhaps the animals changing their orientation and thus decreasing their acoustic reflectivity cannot be distinguished from this analysis.

It therefore seemed reasonable to assume that the animals' motion relative to the sonar system could be regarded as a mean displacement, due to the mean current, $<\bar{v}>$, plus some small
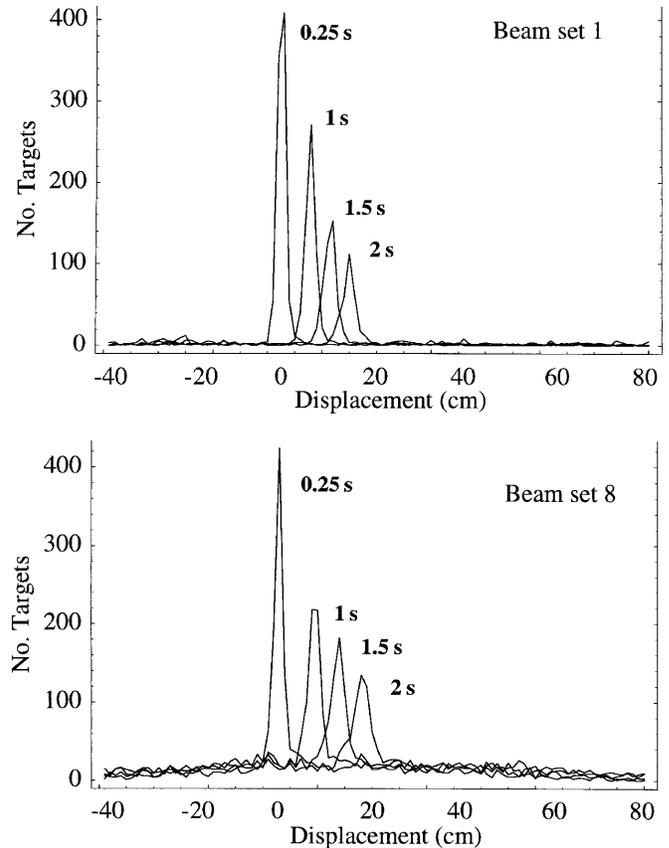
changes, $\Delta\bar{v}$, due to a combination of the animals' movements and turbulent motions so that the total movement is $<\bar{v}>+\Delta\bar{v}$. Figure 2 shows the results from a simulation designed to illustrate the basic concept behind this method. The figure depicts the trajectories of 100 particles whose velocities are the sum of a uniform component and a random component. The starting position of each particle was chosen so that the particles were uniformly distributed in a 10 × 10 unit area centered on the origin. Next, each particle was displaced by an amount that was the superposition of a uniform flow to the right and a random component. The uniform flow was 1 unit per time interval and the random component was normally and isotropically distributed in the plane with a standard deviation of 0.25 unit per time interval. A single random component displacement was chosen for each particle, evaluated at $\Delta T = 1$. This same random displacement was then applied four times to each particle (once for each time delay) and added to the uniform flow. The four vector figures (Figs. 2*a*–2*d*) show the displacements of the particles (from $T = 0$) at different time intervals. Figure 2*e* depicts a histogram of the total particle displacement (relative to $T = 0$) as a function of delay time for the set of 100 particles. The translation of the peak to the right is due to the mean current, while the spreading of the peaks with increasing time delay is due to the uncorrelated motions of the targets and thus estimates the animals' true swimming velocities.

Because movement of the animals can be most accurately measured in the range direction, a technique was developed to obtain a statistical characterization of the animals' three-dimensional mo-

2004

Can. J. Fish. Aquat. Sci. Vol. 56, 1999

tions from these range fluctuations after subtracting out the mean flow $<\bar{v}>$. Under the assumption that the animals' movements are isotropic, changes in range can be regarded as one component of a three-dimensional distribution function. The remainder of this section describes an algorithm that yields an estimate of this distribution function from the range data.

Mathematical algorithm

The algorithm described in this section was designed to yield an estimate for the probability density function for animal velocities, pdf(v). This function describes the animal population with respect to the motion of the animals under the assumptions of temporal and spatial stationarity over the observation time. The procedure is simplified by assuming that the function does not change as a function of orientation, i.e., it is isotropic. Therefore, every one of the individual sonar beams should be measuring approximately the same displacements. By tracking animal displacements in the same beam for different time intervals, a displacement distribution function is obtained, $\mathrm{ddf}_1(\Delta x, \Delta T)$, which is the number of animals that underwent displacement Δx for a fixed delay time ΔT. We use the notation "ddf" to denote that this function is not strictly a probability density function. Under the assumption of isotropy, there is a straightforward relationship between this function and the true three-dimensional displacement distribution function $\mathrm{ddf}_3(\Delta x, \Delta T)$, which can be used to estimate this true distribution function from the measured data for each time delay. Although this function could then be used to directly estimate the pdf(v), a slightly different procedure is used here to obtain this function. Instead, the rate of spreading of this displacement function yields a more accurate estimate for the animal movements than the observation of the individual displacement distribution functions because it takes into consideration the accuracy of the system in localizing animals. Using the set of time-delayed displacement functions, the standard deviation of each one is computed as an estimation of the width of the peak, and then, a straight line is fitted to the set of standard deviations as a function of time delay. The slope of this line, equal to the rate of the spreading of the standard deviation, provides a measure of the function width for pdf(v).

The starting data for the estimation procedure is a set of matrices of sonar backscatter intensity from a single deployment. We use a procedure called "trimming" to identify regions of local maximum backscatter and then trim out the surrounding area, which can have large values of backscatter due to the side lobes of the reflected sound. The procedure is as follows: first, the backscatter matrix is inspected to find its maximum value. Next, after applying a correction for range spreading, attenuation, and calibration of the system, the target strength of this maximum value and its location in three dimensions are computed. Since the beam patterns from our system result in some spreading of the sound into the adjacent volume (mostly in the azimuth), the volume immediately surrounding the identified target is excluded from consideration in finding more targets. The subsequent matrix is inspected for the next highest value and this procedure is repeated until a user-specified target strength (lower bound) is reached. At the end of this procedure, a list of target positions and target strengths is available as a function of frame number for a single set of acoustic reflections.

The list of target strengths is then truncated to the 20 strongest targets per frame that are compatible with measured target strengths of adult euphausiids from the OASIS system (Jaffe et al. 1998). For the most part, these target strengths are associated with adult animals of 15–20 mm total length (–78 dB < TS < –71 dB).[2] Using only the largest animals increased the chances of detection from frame to frame while minimizing the chances of mixing different animals in consecutive positions in sequential frames. These

Fig. 5. Simulation illustrating the relationship between a set of 50 000 three-dimensional translations and the actual one-dimensional projections that are measured by the system. (*a*) The three-dimensional translations are all of the same magnitude, x', however isotropically oriented. (*b*) Values that would be measured by projecting this set of three-dimensional vectors onto a single one-dimensional vector, corresponding to the actual range measurements that the sonar would be making.
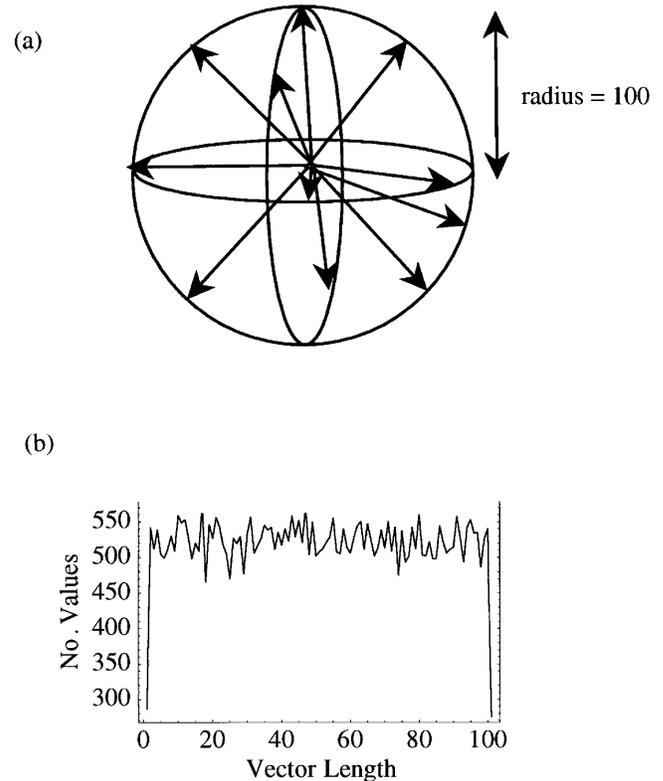
truncated target lists were then processed to obtain an estimate for a one-dimensional probability distribution function of displacements as a function of delay time, $\mathrm{ddf}_1(\Delta x, \Delta T)$, by computing the changes in range between all of the sets of 20 targets between frames for a given time delay ΔT.

To increase the probability that the same animal is being considered, the displacement values were used only if the target stayed in the same beam for the pair of frames that were under consideration. These difference matrices were integrated over all of the frames for a single set of data and then binned to provide the number of targets that underwent displacement Δx for time interval ΔT. At the end of this stage of processing, a set of one-dimensional displacement distribution functions for displacement as a function of delay time were obtained.

The geometric arrangement for the deployment, showing the grouping of the 64 beams into eight sets of eight beams, is illustrated in Fig. 3. Beam set 8 was oriented the most horizontally (declined at 19° from horizontal) and beam set 1 was oriented the most vertically (declined at 33°). The density displacement functions $\mathrm{ddf}_1(\Delta x, \Delta T)$ for beam set 1 and beam set 8 for one of the runs are shown in Fig. 4. The figure illustrates several features of the data sets as follows. (*i*) The mean displacement of the peak increases with time delay between frames due to the mean current. The slope of the relationship between mean displacement and time

---

[2] Our previous paper, which documented the first use of the OASIS system (Jaffe et al. 1998), contains a calibration error: all target strengths reported in that paper were overestimated by 6 dB.

Table 1. Estimated swimming speeds of *E. pacifica* from six deployments in Saanich Inlet, B.C.

Date	Time	Depth (m)	Estimated swimming speed (cm·s^{-1})	SD (cm·s^{-1})
29 July 1997	18:10–18:13	80	0.3	0.23
31 July 1997	16:05–16:09	80	0.9	0.40
8 August 1996	10:11–10:17	80	1.0	0.21
12 August 1996	10:49–10:57	85	1.2	0.43
13 August 1996	11:07–11:15	90	1.1	0.28

Note: Swimming speeds are estimated from the rate of spreading of animal displacement distributions. Standard deviations of swimming speeds are estimated from numerical simulations that computed the resultant standard deviations in the estimated swimming speeds by performing the linear inversion process 10 000 times using the observed standard deviation among the beam sets as an estimate for the true standard deviation of the data.

delay approximates the mean current speed. (*ii*) The width of the peak increases as a function of delay time, due to the dispersion in the measured positions of the animals. This spread in the peak width approximates the swimming speed of the animals. (*iii*) The beam set pointing most horizontally, beam set 8, undergoes a larger mean displacement than beam set 1 because the horizontal projection of the mean current vector was slightly larger than for beam set 1. (*iv*) The widths of the distribution functions for the more horizontally oriented beams were slightly wider than for the more vertically oriented ones (this point will be discussed in more detail below).

The next step was to compute an estimate of the three-dimensional displacement distribution functions, ddf$_3$($\Delta x,\Delta T$), from the one-dimensional displacement distribution function, ddf$_1$(Δx, ΔT), by applying a linear transformation. Although the details of the transformation are provided in the Appendix, the motivation for its use is described here. As an example of one particularly peculiar case, consider a center point of location {0,0,0} as shown in Fig. 5 and the simulated set of 50 000 isotropic displacements of fixed distances $\Delta x'$. Because the methodology here makes use of only the range dimension, the relationship of the range data to the true three-dimensional data needs to be considered. The set of three-dimensional locations {x_i,y_i,z_i} are "projected" onto the axis of the sonar beam, yielding a set of displacement distances (Fig. 5b). The figure illustrates the somewhat curious result that the projection of the set of three-dimensional displacements of an isotropic and single-valued displacement onto one axis results in a constant function. Theoretical analysis of the problem (not presented here) validated this numerical result. Evidently, the result of projecting this three-dimensional distribution onto a one-dimensional beam direction has resulted in a distortion of the probability density function. Since this projection operator is essentially an inner product between the displacement vectors and the beam direction, it is a linear transformation. Moreover, since any one-dimensional observed distribution is a sum of a set of these simple displacement distributions, a linear transformation can be formulated that describes the forward problem. In principle, inversion for the true three-dimensional distribution function from these one-dimensional observations can then be performed. The Appendix contains a proof that the animal displacements are approximately a projection of the displacements, as well as an example of the projection of a normal distribution and an explanation of the inversion technique that was used to obtain an estimate of the three-dimensional displacement density functions from the one-dimensional observations. Four examples of the transformation from ddf$_1$($\Delta x,\Delta T$) to ddf$_3$($\Delta x,\Delta T$) are displayed in Fig A2 in the Appendix.

Although the resultant three-dimensional displacement probability density functions could simply be averaged together to obtain an estimate for the velocity distribution (after dividing through by time), an additional step was added to provide a more accurate estimate of the animal motion. The motivation for its implementation comes from the following reasoning: even though the system can measure range accurately, the measurement of displacement is still subject to a myriad of environmental effects. Fluctuations in animal orientation for animals that subtend more than one range bin, rotation of the sonar system about the suspension wire, and other small instrumental motions are all examples of factors that can degrade the range displacement resolution of the system. Any spreading of the displacement distribution as a function of time would then be superimposed on these more systematic changes. For this reason, the approach taken here attempted to estimate and subtract these motions.

To obtain an estimate for the displacement resolution of the system, the peak widths of the set of three-dimensional displacement distribution functions were computed. Next, a linear fit of the peak width as a function of time delay was obtained. Both the slope and the intercept were computed. The slope of this curve, equal to the value at a 1-s delay with the systematic delay subtracted off, was then used to estimate the true peak width of the animal probability density function for velocity. So, for example, if the measured peak width is pw$_{meas}$ and the true peak width is pw$_{true}$, then the effect of animal motion leads to a linear spreading of this distribution so that

$$pw_{meas} = pw_{spread\ rate} \times time + sd_{offset}$$

where sd$_{offset}$ is the intercept of the linear function at time delay zero. The slope at 1-s delay is thus equal to pw$_{meas}$ − sd$_{offset}$, which is assumed to approximate the true animal distribution (pw$_{true}$). So, for example, if the animals were not moving but the instruments were still subject to the environmental effects, a set of identical displacement probability density functions of some finite width would be observed. In this case, since the standard deviations of the set of displacement probability density functions would not change, the slope of a plot of standard deviation versus delay time would be zero, leading to the correct inference of no animal movement. This procedure assumes that the broadening of the animal displacement function can be viewed as a linear process and that it makes sense to simply subtract out the extrapolated zero time delay value. A more complete treatment would likely involve more sophisticated linear inverse theory; however, the essential results of this analysis would probably not change.

Results

The acoustic returns from six sessions where the sonar was deployed at a fixed depth in the daytime were processed by the algorithms described above. These resulted in the estimation of animal positions in three dimensions, the computation of the one-dimensional displacement density functions, the inversion for the three-dimensional distribution functions, and an estimation of the width of those distributions (the latter approximated by their standard deviation). To address variability of estimated swimming speeds, the individual beam sets were not combined until the last stage of the data pro-

2006

Can. J. Fish. Aquat. Sci. Vol. 56, 1999

Fig. 6. Relationship between oxygen consumption rate and swimming speed for *E. pacifica* (redrawn from Torres and Childress 1983). Measurements were made at 8°C and 1 atm pressure (101.325 kPa) in the daytime, but animals were cycled to 12°C at night while held in the laboratory prior to experiments.
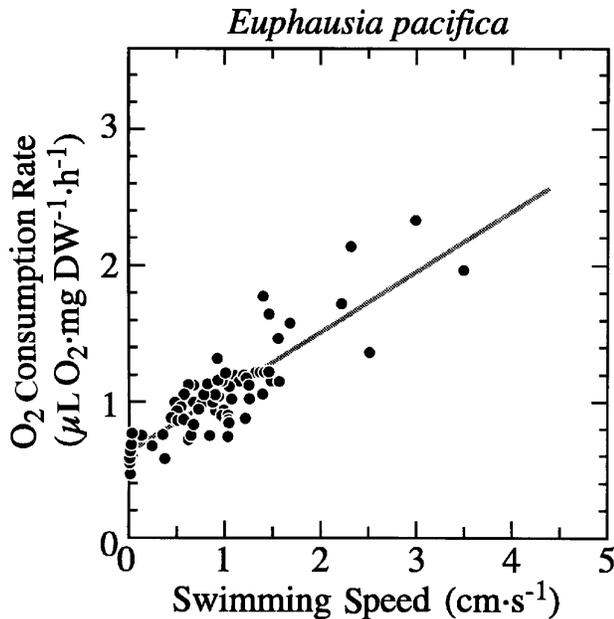
cessing. In this way, an estimation of beam-to-beam consistency of the spread in peak widths for a single run was possible.

The results from analysis of the six data sets are listed in Table 1. In all cases the average speed of the animals, as estimated by the standard deviation, was quite low. It ranged from 0.3 to 1.2 cm·s^{-1}. In order to estimate the variability associated with these mean speeds, a Monte Carlo approach was employed. First, the standard deviations for the set of peak widths were computed for a given delay time and deployment by comparing the peak widths from the eight beam sets. Next, random numbers were drawn from a normal distribution which used the observed mean peak width as an estimate of the true mean peak width and the observed standard deviations among the beam sets as an estimate of the true standard deviation of the estimated swimming speed estimates. Then, the slope of the line of peak width versus delay time was computed. This linear inversion was then repeated 10 000 times for each realization of the four peak widths as a function of delay time. These values are all less than the mean values, indicating relatively little variability among the beam sets in estimating swimming speeds. In addition, the intercept of the straight line fitted to peak width as a function of time delay estimated the systematic delay or the ability of the system to resolve animals positions. These values ranged from 0.02 to 1.2 cm.

Cumulative distribution functions were calculated for a few of the data sets. The purpose of this analysis was to see what fraction of the animals were moving at speeds within one standard deviation from the mean total displacement. Consistent with the distributions being approximately Gaussian, between 60 and 70% of the animals were moving less than or equal to this value.

Discussion

The most striking feature of the estimated swimming speeds of euphausiids reported here is their low values compared with previously reported values. Sustained pleopod swimming speeds of euphausiids from measurements made in aquaria (Hanmer 1984; Price 1989; Land 1992) and in situ estimates (Hanamura et al. 1984; M.D. Ohman, unpublished data) when scaled to body length range from 0.7 to 5 body lengths·s^{-1}. Because the swimming speeds observed in this study (0.5–1 body lengths·s^{-1}) are at the lower end of this range and are low in absolute units (0.3–1.2 cm·s^{-1}), we infer that *E. pacifica* exhibits quiescent behavior with limited motion in subsurface waters during the daytime.

While not surprising, these results provide the first direct evidence for markedly reduced swimming activity of diel migrant euphausiids at their daytime depths. This behavior has at least two adaptive advantages over the alternative of sustaining swimming activity in deeper strata. First, the reduction of swimming velocity will reduce encounter rates with most types of predators, especially ambush predators (e.g., Gerritsen and Strickler 1977). Second, reduced motility is an energetically efficient behavior that decreases metabolic costs.

This reduction in metabolic cost as a consequence of reduced swimming activity at depth should not be confused with once-hypothesized metabolic advantages of diel vertical migration behavior, a long-abandoned (McLaren 1974) argument for zooplankton diel vertical migration. Torres and Childress (1983), in the best experiments to date addressing the metabolic costs of swimming in euphausiids, discovered that there is more than a threefold increase in metabolic rate as *E. pacifica* increases its rate of swimming (see Fig. 6, redrawn from their study). Work on zooplankton metabolism prior to these authors often arrived at different conclusions because of the authors' failure to distinguish between basal metabolism (animals at rest) and routine metabolism (animals spontaneously active). When this distinction is made properly and resolved experimentally, the rate of oxygen consumption varies steeply with the activity level of the animals (Fig. 6), conferring considerable energetic benefit on quiescent behavior. Conversely, as Torres and Childress (1983) pointed out, the increase in swimming speed when animals migrate vertically results in substantial metabolic costs that nullify any hypothetical metabolic savings of diel vertical migration for euphausiids. The adaptive value of diel vertical migration for euphausiids, as for other zooplankton (Ohman 1990; Bollens et al. 1994), generally concerns the minimization of predation risk. Substantial energetic costs associated with locomotion have been demonstrated in planktonic mysids (Buskey 1998*a*), lophogastrids (Cowles and Childress 1988), and planktonic copepods (Buskey 1998*b*).

The velocities that we have measured from the rate of spreading of animal displacements as a function of time delay are the uncorrelated velocities between pairs of acoustic reflectors. These velocities actually include two sources of motion: the swimming motions of the animals and an unknown contribution of turbulent fluid motions. We are not able to resolve the relative contributions of these two sources. However, our result is not affected by this ambiguity. In the extreme case of no turbulent motions, all of the observed displacement would be caused by swimming,

which leaves the motion remarkably small. In the other extreme, if all the motion were due to turbulent velocity fluctuations in the fluid, the animals would be absolutely stationary in the daytime, further reinforcing our result.

We tested our assumption of isotropic swimming motions by analyzing three-dimensional swimming vectors of euphausiids using a target-tracking algorithm. These results showed that the euphausiids in this study site exhibit nearly isotropic swimming behavior at most times (A. De Robertis, unpublished observations). An exception occurs at the times of peak vertical flux during diel vertical migrations, when animal displacements are highly directional, but such intervals are not relevant here. Furthermore, any small departure from isotropy would likely cause us to overestimate the mean swimming speeds. Since the acoustic beams are oriented just off the horizontal axis and we rely on the higher sonar resolution in the range dimension, if the euphausiids were swimming mainly in the horizontal plane to maintain themselves at a constant depth, our emphasis on the horizontal swimming velocities would cause us to overestimate (not underestimate) the true swimming speeds.

Another possible source of error arises if currents are not constant during the time intervals over which the displacement distribution functions are calculated. Rapidly fluctuating currents would cause peak widths to broaden with increasing time delays, which would also lead us to overestimate the behavioral component of swimming velocities to some extent. Hence, any bias introduced by this factor would also lead us to report maximal daytime swimming velocities.

Our assumption that the swimming movements of euphausiids are uncorrelated implies that there is no significant schooling behavior. While *Euphausia superba* in the Antarctic is well known to form coherent schools (e.g., Hamner et al. 1989) and *E. pacifica* has been reported to form groups with parallel orientation at the sea surface in the Sea of Japan (Komaki 1967; Hanamura et al. 1984), we are not aware of any reports of daytime schooling behavior of *E. pacifica* in the vicinity of Saanich Inlet. Mackie and Mills (1983) observed dense aggregations of up to 10 000 animals·m^{-3} in very thin vertical layers above the oxycline in Saanich Inlet but made no remarks suggesting that these animals were arranged in schools with similar orientation and coordinated swimming motions.

Various other aspects related to the data processing and estimation merit discussion. Distances between the 20 strongest targets in each of the successive frames were used because this increases the likelihood of tracking the same set of targets from frame to frame. If the 20 strongest targets are even moderately uniformly distributed within the sonar volume, the closest target to a given target between frames should be the very same target. Figure 1 illustrates that the sonar records contain the reflections from many targets that are strong and can be followed from frame to frame. In addition, inspection of the target lists showed that there were many targets that were clearly identifiable and either drifting or moving very slowly. At longer frame delays (4 s was the maximum delay used) the possibility of mistaking target trajectories becomes more probable unless a specific target-tracking algorithm is use. As applied, our procedure provided reasonable estimates for both the current velocity and

the spreading of the animal displacement distribution functions.

Consideration of the bias produced by requiring the animal to stay in the same beam is also an important question. Since the target identification procedure only recognizes targets that have stayed in the same beam, it is possible that the faster moving targets could be missed. Targets that are transiting from one beam to another will also be missed. In order to judge the effects of this potential source of bias, a computer simulation was performed. The simulation placed a set of targets inside a volume with the approximate dimension of one of the insonified beams. Next, the targets were translated with a displacement that was the sum of a mean component plus a random component. The random component was an isotropic and normally distributed displacement function, designed to approximate the movement of the animals. The mean component was a uniform translation that was designed to approximate the effect of current. The relative angles between the beam and current were chosen so that the beam corresponded to the most downward pointing one. This beam would induce the maximum amount of narrowing of the displacement distribution function, as compared with the other beams, since the targets spend the least amount of time in it. The mean component was chosen to simulate a current of 7 cm·s^{-1} (the maximum current observed in the first year) and the random component was drawn from a normally distributed probability density function for velocity that was isotropic in angle with standard deviations of 0.25, 0.5, 1, 2, and 3 cm·s^{-1}. The total displacements were chosen to correspond to a tracking time of 2 s, identical to the tracking time for the experiments performed in the first year. The simulations indicated that a 10% narrowing of the displacement distribution functions should be expected. Since this beam is a worst case, we conclude that the bias introduced by the finite residence time of the particles in a single beam, with the faster moving particles "jumping" out, is of only minor significance.

The simulations also explain why, in Fig. 4, the displacement distribution functions from beam set 8 are somewhat wider than those of beam set 1, with an increasing discrepancy with increasing delay time. The targets in beam set 8 have a longer residence time because the current flow is mainly horizontal and this beam is more horizontally oriented than the rest. The longer residence time leads to a somewhat wider distribution function, as evidenced in the computer simulations, as the particles that are more active do not jump out of the beam with the same frequency as the particles that are in the beams that are pointing more vertically.

Studies of the in situ behavior of zooplankton have been constrained by the limited number of tools available (see Sprules et al. 1992). Many approaches introduce observer effects through intrusive lighting or hydrodynamic disturbances. Although direct SCUBA observations (e.g., Hamner 1984) have been invaluable, they are limited to a very shallow sector of the water column. The present results illustrate the utility of tracking sonar systems, especially when combined with optical verification of the identity of targets (Jaffe et al. 1998), for investigating the behavior of zooplankton in their natural environment. This permitted us to measure, for the first time, the quiescent swimming behavior of euphau-

siids in daytime strata. Reduced motility confers simultaneous advantages of reduced metabolic costs and minimization of encounter rates with predators.

Acknowledgments

References

Andersen, V., and Nival, P. 1991. A model of the diel vertical migration of zooplankton based on euphausiids. J. Mar. Res. **49**: 153–175.

Boden, B.P., and Kampa, E.M. 1965. An aspect of euphausiid ecology revealed by echo-sounding in a fjord. Crustaceana, **9**: 155–173.

Bollens, S.M., Frost, B.W., and Cordell, J.R. 1994. Chemical, mechanical and visual cues in the vertical migration behavior of the marine planktonic copepod *Acartia hudsonica*. J. Plankton Res. **16**: 555–564.

Brinton, E., Ohman, M.D., Townsend, A.W., Knight, M.D., and Bridgeman, A.L. 1999. Euphausiids of the World Ocean. CD-ROM, ETI, University of Amsterdam, Amsterdam, The Netherlands. 586 megabytes.

Buskey, E.J. 1998*a*. Energetic costs of position-holding behavior in the planktonic mysid *Mysidium columbiae*. Mar. Ecol. Prog. Ser. **130**: 139–147.

Buskey, E.J. 1998*b*. Energetic costs of swarming behavior for the copepod *Dioithona oculata*. Mar. Biol. **130**: 425–431.

Buskey, E.J., Coulter, C., and Strom, S. 1993. Locomotory patterns of microzooplankton: potential effects on food selectivity of larval fish. Bull. Mar. Sci. **53**: 29–43.

Cowles, D.L., and Childress, J.J. 1988. Swimming speed and oxygen consumption in the bathypelagic mysid *Gnathophausia ingens*. Biol. Bull. **175**: 111–121.

Gerritsen, J., and Strickler, J.R. 1977. Encounter probabilities and community structure in zooplankton: a mathematical model. J. Fish. Res. Board Can. **34**: 73–82.

Hamner, W.M. 1984. Aspects of schooling in *Euphausia superba*. J. Crustacean Biol. **4**(Spec. No. 1): 67–74.

Hamner, W.M., Hamner, P.P., Obst, B.S., and Carleton, J.H. 1989. Field observations on the ontogeny of schooling of *Euphausia superba* furciliae and its relationship to ice in Antarctic waters. Limnol. Oceanogr. **34**: 451–456.

Hanamura, Y., Endo, Y., and Taniguchi, A. 1984. Underwater observations on the surface swarm of a euphausiid, *Euphausia pacifica* in Sendai Bay, northeastern Japan. Mer (Tokyo), **22**: 63–69.

Jaffe, J.S., Reuss, E., McGehee, D., and Chandran, G. 1995. FTV, a sonar for tracking macrozooplankton in three-dimensions. Deep-Sea Res. **42**: 1495–1512.

Jaffe, J.S., Ohman, M.D., and De Robertis, A. 1998. OASIS in the sea: measurement of the acoustic reflectivity of zooplankton with concurrent optical imaging. Deep-Sea Res. **45**: 1239–1253.

Kak, A.C., and Slaney, M. 1987. Principles of computerized tomographic imaging. IEEE Press, New York.

Komaki, Y. 1967. On the surface swarming of euphausiid crustaceans. Pac. Sci. **21**: 433–448.

Land, M.F. 1992. Locomotion and visual behaviour of mid-water crustaceans. J. Mar. Biol. Assoc. U.K. **72**: 41–60.

Mackie, G.O., and Mills, C.E. 1983. Use of the *Pisces IV* submersible for zooplankton studies in coastal waters of British Columbia. Can. J. Fish. Aquat. Sci. **40**: 763–776.

McGehee, D., and Jaffe, J.S. 1996. Three-dimensional swimming behavior of individual zooplankters: observations using the acoustical imaging system FishTV. ICES J. Mar. Sci. **53**: 363–369.

McLaren, I.A. 1974. Demographic strategy of vertical migration by a marine copepod. Am. Nat. **108**: 91–102.

Ohman, M.D. 1990. The demographic benefits of diel vertical migration by zooplankton. Ecol. Monogr. **60**: 257–281.

Price, H.J. 1989. Swimming behavior of krill in response to algal patches: a mesocosm study. Limnol. Oceanogr. **34**: 649–659.

Sprules, W.G., Schulze, P.C., and Williamson, C.E. 1992. Advanced techniques for in situ studies of zooplankton abundance, distribution, and behavior. Arch. Hydrobiol. Beih. Ergebn. Limnol. **36**: 1–140.

Torres, J.J., and Childress, J.J. 1983. Relationship of oxygen consumption to swimming speed in *Euphausia pacifica*. 1. Effects of temperature and pressure. Mar. Biol. **74**: 79–86.

Appendix

An animal displacement of Δr in a single sonar beam is illustrated in Fig. A1. It is necessary to show that the "projection" of this vector onto the axis of the beam Δr_b is what is measured by the sonar. Existing methods to reconstruct functions from their projections can then be invoked (Kak and Slaney 1987). The animal's initial position is $d\bar{1}$, and after a short time, the animal is at position $d\bar{2}$, where $d\bar{1}$ and $d\bar{2}$ are vectors and the transducer is located at the origin of the coordinate system. Since in this analysis, we measure only range, the displacement measured by the sonar is $|d\bar{2}| - |d\bar{1}|$. However, since the vector $\Delta r_b = d\bar{2} \cos \Theta - d\bar{1}$, this is approximately equal to $|d\bar{2}| - |d\bar{1}|$, since these vectors are colinear and $\cos \Theta$ is approximately equal to 1 (0.9998) for a maximum angle of 1°, which is the half-angle that the beam subtends. Thus, at a range of 10 m, the maximum discrepancy that is possible with this approximation is 2 mm, far below the range resolution of the system.

Fig. A1. Geometric projection of the true three-dimensional displacement onto the range axis of the sonar beam.
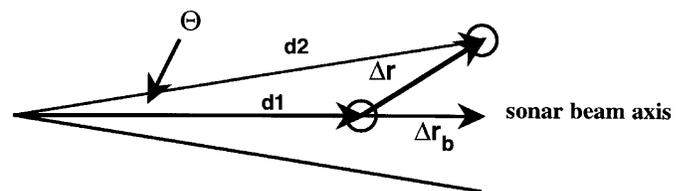
As an example, consider a set of animal displacements that are normally distributed in three dimensions with mean zero and variance σ. The three-dimensional probability density function of the displacements can be represented as

$$(A1) \quad f(\Delta x, \Delta y, \Delta z) = \frac{1}{2\pi\sigma^2} e^{-\frac{\Delta x^2 + \Delta y^2 + \Delta z^2}{2\sigma^2}}.$$

Fig. A2. Illustration of a set of displacement distribution functions before and after processing that allow the computation of $ddf_3(\Delta x, \Delta T)$ from $ddf_1(\Delta x, \Delta T)$.

$ddf_1(\Delta x, \Delta T)$

$ddf_3(\Delta x, \Delta T)$
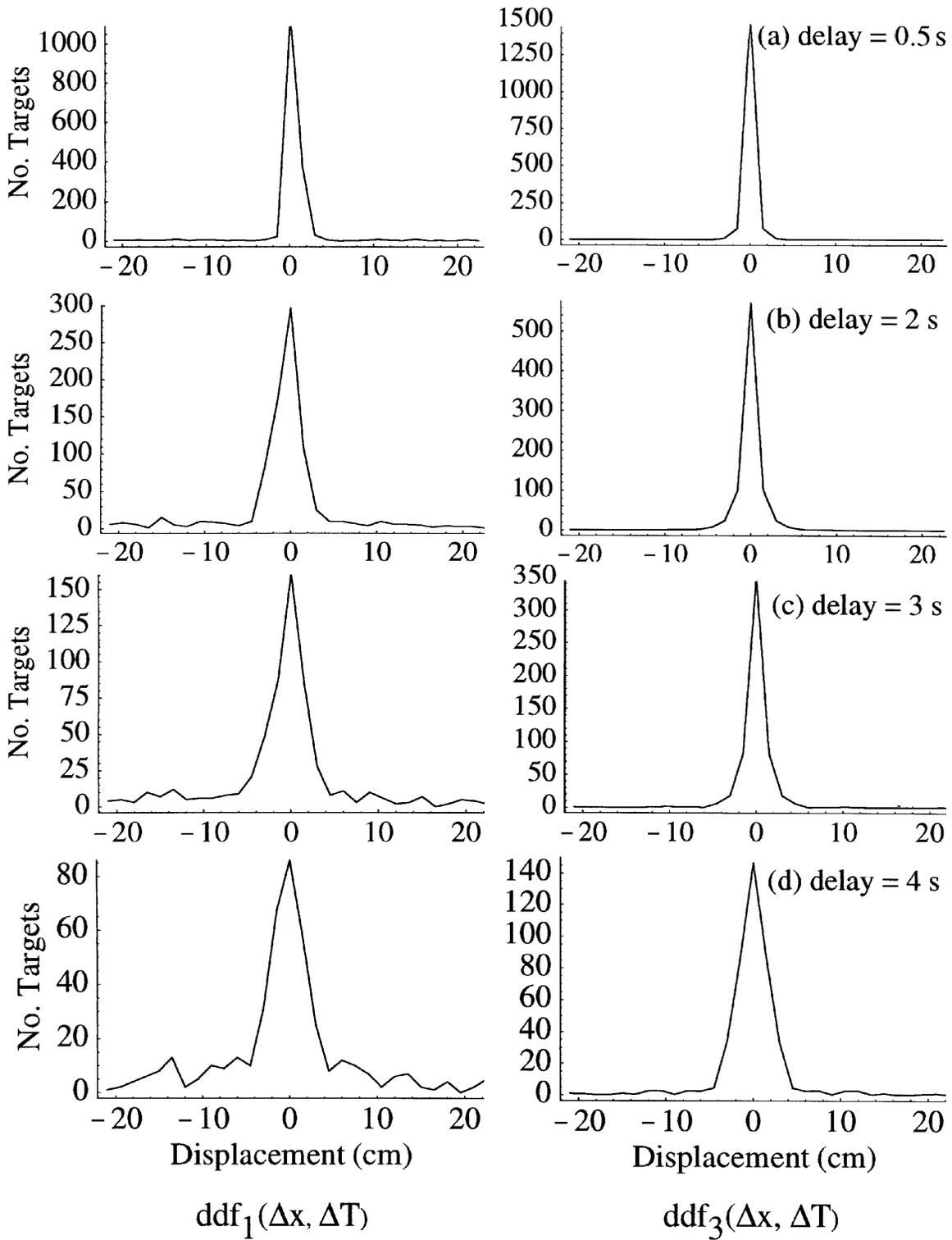
In this case, the projection of this function onto a one-dimensional axis (here taken to be the y-axis with no loss of generality, since this function is isotropic) is the marginal probability distribution function

(A2) $\quad f(\Delta y) = \int\int \dfrac{1}{2\pi\sigma^2}\, e^{-\frac{\Delta x^2 + \Delta y^2 + \Delta z^2}{2\sigma^2}}\, dxdz$

which is equivalent to

Can. J. Fish. Aquat. Sci. Vol. 56, 1999

$$(A3) \quad f(\Delta y) = \frac{1}{2\pi\sigma^2} \, e^{-\frac{\Delta y^2}{2\sigma^2}}.$$

Evidently, since the projection of this normally distributed function onto a single axis results in a normally distributed function with equal variance, there is no need to invert for the "true" three-dimensional function.

Now, since the displacement distribution function is a sum of projected functions, via the linearity of the projection operator, it can be shown that the measured one-dimensional displacement distribution is a projection of the true three-dimensional displacement distribution function. Thus, inversion of the measured one-dimensional displacement distribution is what is desired. We present without proof here the necessary algorithm and refer the interested reader to the tomography literature (Kak and Slaney 1987) for details.

Given the one-dimensional displacement distribution function $\mathrm{ddf}_1(\Delta y, \Delta T)$, the inversion can be accomplished via a one-dimensional Fourier transform $\mathcal{F}$ followed by a three-dimensional inverse Hankel transform $\mathcal{H}^{-1}$:

$$(A4) \quad \mathrm{ddf}_3(\Delta y, \Delta T) = \mathcal{H}^{-1}\{\mathcal{F}[\mathrm{ddf}_3(\Delta y, \Delta T)]\}$$

In order to implement this scheme, a computer algorithm was written in Mathematica (Wolfram, Ill.). The performance of the algorithm was verified for several sets of test data (normally distributed functions). Figure A2 demonstrates a set of displacement distribution functions before and after transformation. Some narrowing of the functions can be noted after transformation, which indicates that the functions are approximately but not strictly normal distributions.

© 1999 NRC Canada